Eur. Phys. J. B **61**, 475–483 (2008)
DOI: 10.1140/epjb/e2008-00093-1

THE EUROPEAN PHYSICAL JOURNAL B

Lifting the singular nature of a model for peeling of an adhesive tape

R. De[1,a] and G. Ananthakrishna[2,b]

[1] Department of Materials and Interfaces, Weizmann Institute of Science, Rehovot, 76100 Israel
[2] Materials Research Centre and Centre for Condensed Matter Theory, Indian Institute of Science, Bangalore-560012, India

Received 24 June 2007 / Received in final form 10 December 2007
Published online 5 March 2008 –

Abstract. We investigate the dynamics of peeling of an adhesive tape subjected to a constant pull speed. Due to the constraint between the pull force, peel angle and the peel force, the equations of motion derived earlier fall into the category of differential-algebraic equations (DAE) requiring an appropriate algorithm for its numerical solution. By including the kinetic energy arising from the stretched part of the tape in the Lagrangian, we derive equations of motion that support stick-slip jumps as a natural consequence of the inherent dynamics itself, thus circumventing the need to use any special algorithm. In the low mass limit, these equations reproduce solutions obtained using a differential-algebraic algorithm introduced for the earlier singular equations. We find that mass has a strong influence on the dynamics of the model rendering periodic solutions to chaotic and vice versa. Apart from the rich dynamics, the model reproduces several qualitative features of the different waveforms of the peel force function as also the decreasing nature of force drop magnitudes.

PACS. 5.45.-a Nonlinear dynamics and chaos – 68.35.Np Adhesion – 02.90.+p Solution of differential-algebraic equation

1 Introduction

The phenomena of adhesion has attracted attention due to scientific challenges it poses as well as for their industrial importance. Science of adhesion is truly interdisciplinary involving a great variety of different interrelated physical phenomena like friction, fracture, mechanics of contact, visco-plastic deformation and interfacial properties such as debonding and rupture of adhesive bonds. Detailed mechanisms of such a complicated mixture of phenomena are not yet well understood.

Tests of adhesion are essentially fracture tests designed to study adherence of solids and generally involve normal pulling off and peeling. Peeling also provides a rich insight into fracture mechanics as the dynamics is highly nonlinear and shows a variety of instabilities and complex structures. Furthermore, peeling experiments are comparatively easy to setup in laboratory and the recorded response helps to extract useful information on the nonlinear features of the system.

The first detailed experimental study on peeling of an adhesive tape was due to Maugis and Barquins [1]. These experiments carried out at constant pull speed condition show that peeling is jerky within a window of pull speeds accompanied by acoustic emission [2,3]. Constant load experiments have also been carried out recently [4,5]. The experimental strain energy release rate G shows two stable branches separated by an unstable branch. At low applied velocities, the peeling front keeps pace with the pull velocity and the failure mode is cohesive whereas at high pull velocities, the failure is adhesive. If the pull speed is within some intermediate range, one sees stick-slip oscillations. These authors report that the pull force shows a rich variety of behavior ranging from sinusoidal, sawtooth and highly irregular (chaotic as these authors refer to) wave patterns with increasing pull speeds [1]. They also report that the average amplitude of the pull force decreases with increasing pull speeds.

Apart from detailed experimental investigation of the peeling process, Maugis and Barquins [1], have also contributed substantially to the understanding of the dynamics of the peeling process by writing down preliminary set of equations relevant for the experimental situation and carrying out dynamical analysis of the equations under certain approximations [1]. Indeed, Maugis identifies Hopf bifurcation as the cause of stick-slip oscillations [1,6]. Hong and Yue [7] modified these equations and carried out a dynamical analysis using an 'N' shaped function to mimic the dependence of the peel force on the rupture speed. They reported that the system of equations exhibits periodic

[a] e-mail: rumi.de@weizmann.ac.il
[b] e-mail: garani@mrc.iisc.ernet.in

and chaotic stick-slip oscillations. However, the jumps in the rupture speed were introduced *externally* once the rupture velocity reached the limit of stability [8]. *Thus, the stick-slip oscillations are not obtained as a natural consequence of the equations of motion.* Indeed, the fact that dynamical jumps in the rupture velocity (across the two branches) cannot be obtained from these equations was later recognized by Ciccotti et al. [2]. For this reason, these authors interpret the stick-slip jumps as catastrophes. Recently we derived these equations starting from a Lagrangian and showed [9] that these equations are singular, and fall in the category of differential-algebraic equations (DAE) [10] requiring an appropriate algorithm. Using a DAE algorithm, we showed that stick-slip jumps across the two branches arise in a pure dynamical way. The dynamics was also shown to be much richer than anticipated earlier.

However, even though the DAE algorithm is a nice mathematical framework for obtaining solutions for these singular equations, it is difficult to provide any physical interpretation for the perturbed 'mass matrix' that removes the singularity. *Thus, it is necessary to identify the missing physics responsible for the absence of dynamical jumps in these equations.* Our investigations in this direction show that a time scale corresponding to the kinetic energy of the stretched part of the tape is missing in the original model equations [11]. Using the Lagrange's equations of motion, we derive equations of motion which show that once kinetic energy of the tape is included, the set of differential-algebraic equations are converted to a coupled set of ordinary differential equations (ODE). We shall refer to the modified model as the ODE model. In the limit of zero mass of the tape, i.e., when the inertial time scale of the tape is small, the solutions obtained from the ODE model match that from DAE. The purpose of this paper is to provide a comprehensive comparative study of the ODE solutions and the DAE solutions for the entire range of parameter space, extending the preliminary results published earlier [11]. We shall also comment on the utility of this regularization procedure adopted here to other DAE type of equations.

2 Model

Here we start by considering the geometry of the experimental setup shown schematically in Figure 1. An adhesive roller tape of radius R is mounted on an axis passing through O normal to the paper and is driven by a couple meter motor positioned at O' with constant speed V. The pull force F acting along the line PO' subtends an angle θ at the contact point P. The contact point P moves with a local velocity v which can under go rapid bursts in the velocity during rupture. (We recall here that the peel force function $f(v)$ measured in experiments in steady state conditions goes as an input.) Let the distance from the center of the roller tape O to the motor O' be l. The peeled length of the ribbon, PO' is denoted by L and as peeling point P is not fixed L also changes. The point P subtends an angle α at O, with the horizontal line OO'.

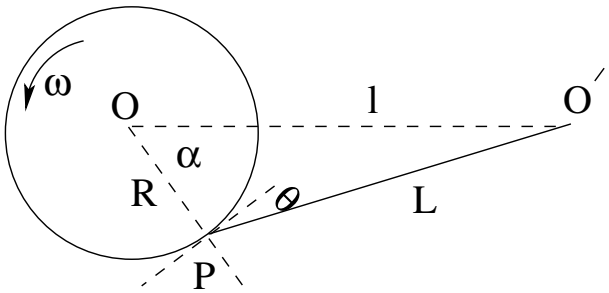

Fig. 1. Schematic plot of experimental setup.

We denote the moment of inertia of the unwinding roller by I, the elastic constant of the adhesive tape by k, the elastic displacement of the tape by u, the angular velocity by ω. As the contact point is not fixed, the angular velocity is identified by $\omega = \dot{\alpha} + v/R$. The geometry of the setup gives $L\cos\theta = -l\sin\alpha$ and $L\sin\theta = l\cos\alpha - R$ which further gives, $L^2 = l^2 + R^2 - 2lR\cos\alpha$. As peeling point P moves, The total velocity V is made up of three contributions [1], given by $V = v + \dot{u} - \dot{L}$, which gives,

$$v = V - \dot{u} + \dot{L} = V - \dot{u} - R\cos\theta\,\dot{\alpha}. \tag{1}$$

Now to derive the equations of motion, we start with the Lagrangian $\mathcal{L} = U_K - U_P$ where U_P is the potential energy of the stretched ribbon and U_K is the kinetic energy of the system given by

$$U_K = \frac{I}{2}\omega^2 + \frac{m}{2}\dot{u}^2, \tag{2}$$

where first term represents the kinetic energy of the roller tape and second term arises due to kinetic energy of the stretched part of the tape [12]. Here, m is the mass of the tape of length L which we shall often refer to as just mass, and I the moment of inertia of the roller tape. The over dot on u refers to the time derivative.

We write the dissipation function as

$$\mathcal{R} = \Phi(v, V) = \int f(v, V)dv, \tag{3}$$

where $f(v, V)$ physically represents the peel force which we assume is dependent on the rupture speed, v, as well as the pull speed, V (see below). Further, $f(v, V)$ is assumed to be derivable from a potential function $\Phi(v, V)$.

The existence of velocity weakening law is quite common to many driven dissipative systems which exhibit stick-slip instability [13], for instance, sliding friction [14] and the Portevin-Le Chatelier (PLC) effect [15–17] to name only two. Indeed, there is a considerable similarity between the PLC effect [15–17] and the peeling problem which has been noted earlier [1]. Briefly, the PLC effect refers to a kind of plastic instability observed when metallic alloys are subjected to constant strain rate deformation. In a range of strain rates and temperatures, stress exhibits different types of serrations with increasing strain rate (or decreasing temperature) that are associated with different types of dislocation bands. The physical mechanism causing different types of serrations and the band

types is the repeated pinning and unpinning of dislocations in solute atmosphere of the alloy. On a macroscopic scale this translates to the negative strain rate sensitivity of the flow stress. This feature which is at the root of the PLC instability is similar to the velocity weakening feature of the peel force function in peeling of an adhesive tape.

More importantly, as in the case of the peeling problem where one finds decreasing amplitude of the peel force drops with increasing pull speed, the amplitudes of the PLC stress drops also decrease with increasing applied strain rate. In the case of the PLC effect, at low strain rate, the plastic relaxation has enough time to come to completion as the time scale of deformations is large. On the other hand at high strain rates, there is insufficient time for plastic relaxation. Thus, the physical cause of this decreasing amplitude of the serrations with applied strain rate has been attributed to incomplete plastic relaxation [16–18]. As demonstrated in reference [18], this amounts to assuming the negative strain rate sensitivity (SRS) of the flow stress $f(\dot{\epsilon}_p)$ to depend, not just on the plastic strain rate $\dot{\epsilon}_p$, but on the applied strain rate, $\dot{\epsilon}_a$ as well. The dependence on $f(\dot{\epsilon}_p, \dot{\epsilon}_a)$ is such that the gap between the maximum and the minimum of the function $f(\dot{\epsilon}_p, \dot{\epsilon}_a)$ decreases with increasing $\dot{\epsilon}_a$ [18]. This has been termed a dynamization scheme to reflect a competition between the time scale of plastic relaxation with the time scale of applied strain rate.

Unlike the PLC effect where a large body of literature exists [16,17] that has been used to understand the underlying mechanisms contributing to the negative strain rate sensitivity of the flow stress, in the case of peeling of adhesives, very little is known about the causes leading to presence of the unstable branch in the peel force function. However, following studies on stick-slip dynamics [13], one can trace the physical origin of the velocity weakening law as arising due to the competition between the internal relaxation time scale of the viscoelastic fluid and the time scale determined by the applied velocity [3]. When the applied velocity is low, there is sufficient time for the viscoelastic fluid to relax. As we increase the applied velocity, the relaxation of the fluid gets increasingly difficult and thus behaves much like an elastic substance.

Following the case of the PLC effect [18], we argue that the effective peel force function should depend on pull velocity. The crucial step is to recognize that the two stable branches of the peel force function correspond to stationary peel situation. However, considering the well known rate dependence of deformation of adhesives, it is clear that when the pull velocity is in the instability domain, the extent of peel and hence the magnitude of the peel force are dynamical quantities. More specifically, the peel bursts are accompanied by loading, unloading and reloading. Considering the frequency dependence of the elastic constant [19], the magnitude of force attained during reloading depends on the extent of viscoelastic relaxation that has occurred during the preceding force drop. This, in principle, would be different for each force drop. Thus, the force seldom reaches the values prescribed by stationary branches. Moreover, an increase in the pull speed amounts to a decrease in viscoelastic relaxation which in turn leads to a reduction in the magnitude of dynamical force. Thus, the peel force function should depend on V also. Using the experimental fact that the magnitude of the force drop decreases toward the end of the instability domain, we modify the peel force function in a way that reduces the gap between maximum and minimum of the effective peel force function. Clearly, in the absence of additional experimental or theoretical support (quite unlike in the PLC effect), there is no unique way to modify the peel force function. We have therefore parameterized the form of $f(v, V)$ so as to decrease the gap between the (dynamic) force maximum and minimum to follow the generally decreasing trend of the force wave form. This is given by

$$\begin{aligned} f(v,V) = {} & 402v^{0.34} + 171v^{0.16} + 68e^{(v/7.7)} \\ & - (415 - 45V^{0.4} - 0.35V^{2.15})v^{0.5} \\ & - 2V^{1.5}, \end{aligned} \tag{4}$$

to depend on the pull velocity V. This form mimics the velocity weakening behavior [1]. Here, it must be stressed that studies on the PLC effect[16,17] as also general stick-slip dynamical systems [13] have demonstrated that the basic features of the stick-slip phenomenon can be recovered without knowing the exact form of $f(v, V)$ as long as $f(v, V)$ contains the velocity weakening branch. One aspect that should be incorporated properly is the extent of velocity bursts. This feature has been included in the above expression.

Using the Lagrange equations of motion,

$$\frac{d}{dt}\left(\frac{\partial \mathcal{L}}{\partial \dot{\alpha}}\right) - \frac{\partial \mathcal{L}}{\partial \alpha} + \frac{\partial \mathcal{R}}{\partial \dot{\alpha}} = 0, \tag{5}$$

$$\frac{d}{dt}\left(\frac{\partial \mathcal{L}}{\partial \dot{u}}\right) - \frac{\partial \mathcal{L}}{\partial u} + \frac{\partial \mathcal{R}}{\partial \dot{u}} = 0. \tag{6}$$

and using $(\alpha, \dot{\alpha}, u, \dot{u})$ as generalized coordinate, we get

$$\ddot{\alpha} = -\frac{\dot{v}}{R} + \frac{R}{I}\frac{\cos\theta}{(1-\cos\theta)} f(v,V), \tag{7}$$

$$m\ddot{u} = \frac{1}{(1-\cos\theta)}[\, f(v,V) - k\,u(1-\cos\theta)]. \tag{8}$$

These equations in their present form are still not suitable for further analysis as they have to satisfy the constraint equation equation (1). In the spirit of classical mechanics of systems with constraints (see Ref. [20]), we derive the equation for the acceleration variable $\dot{v}$ in the constraint equation by differentiating equation (1) as

$$\dot{v} = -\ddot{u} + R\sin\theta\,\dot{\theta}\,\dot{\alpha} - R\cos\theta\,\ddot{\alpha}. \tag{9}$$

Using equations (7), (8) in equation (9) gives

$$\dot{\alpha} = \omega - v/R, \tag{10}$$

$$\dot{\omega} = \frac{R}{I}\frac{\cos\theta}{(1-\cos\theta)} f(v,V), \tag{11}$$

$$\dot{u} = V - v - R\cos\theta\,\dot{\alpha}, \tag{12}$$

$$\dot{v} = \left[\frac{ku}{m} - \frac{f(v,V)}{m(1-\cos\theta)} - \frac{(R\cos\theta)^2 f(v,V)}{I(1-\cos\theta)} + \frac{R}{L}\dot{\alpha}^2(l\cos\alpha - R(\cos\theta)^2)\right]/(1-\cos\theta). \tag{13}$$

3 Differential-algebraic equations and its algorithm

In low mass limit, equation (8) becomes

$$F(1-\cos\theta) - f(v,V) = 0. \tag{14}$$

Then the equations of motion can be written

$$\dot{\alpha} = \omega - v/R, \tag{15}$$

$$\dot{\omega} = \frac{FR}{I}\cos\theta, \tag{16}$$

$$\dot{u} = (V-v) - \cos\theta(\omega R - v), \tag{17}$$

$$0 = F(1-\cos\theta) - f(v,V). \tag{18}$$

These equations were derived and studied by Hong and Yue [7]. Later, these equations have been studied by several authors [2,3] We note that equation (18) is an algebraic constraint that should be respected at all times by the α, ω and u that evolve in time and hence the above set is classified as DAE. Equations (15)–(18) can be written as

$$M\dot{\mathbf{X}} = \xi(\mathbf{X}), \tag{19}$$

where $\mathbf{X} = (\alpha, \omega, F, v)$, ξ is a vector function that governs the evolution of $\mathbf{X}$ and M is a singular "*mass matrix*" [10] given by,

$$M = \begin{pmatrix} 1 & 0 & 0 & 0 \\ 0 & 1 & 0 & 0 \\ 0 & 0 & 1 & 0 \\ 0 & 0 & 0 & 0 \end{pmatrix}.$$

Equation (19) can be solved using the so called singular perturbation technique [10] in which the singular matrix M is perturbed by adding a small constant ϵ such that the singularity is removed. The resulting equations can then be solved numerically and the limit solution obtained as $\epsilon \to 0$ [9].

4 Equations of motion in scaled units

It is a general practice to write all equations of motion in scaled form. To do this, we first identify the basic length and time scales. A natural choice for a time like variable is to use

$$\tau = \omega_u t; \quad \omega_u^2 = k/m. \tag{20}$$

Let, f_{max} be the maximum value of the peel force $f(v,V)$ on the left stable branch. Then, using a basic length scale can be defined by $d = f_{max}/k$, we can define all scaled lengths by $u = Xd$, $l = l^s d$, $L = L^s d$, and $R = R^s d$. The peel force f can be written as

$$f = f_{max}\ \phi(v^s, V^s), \tag{21}$$

where $v^s = v/v_c\omega_u d$ and $V^s = V/v_c\omega_u d$ are the dimensionless peel and pull speeds respectively. Here, $v_c = v_{max}/\omega_u d$ is dimensionless critical velocity at which the unstable branch starts and v_{max} is the maximum value of v in the unscaled variables. In addition, we define $C_f = (m/I)(f_{max}/k)^2$.

Now, ϕ in scaled unit can be written as

$$\phi(v^s,V^s) = \left(\frac{1}{280.8}\right)\Big[402(v_{max}v^s)^{0.34} + 171(v_{max}v^s)^{0.16} - \Big(415 - 45(v_{max}V^s)^{0.4} - 0.35(v_{max}V^s)^{2.15}\Big)(v_{max}v^s)^{0.5} + 68e^{(v_{max}v^s/7.7)} - 2(v_{max}V^s)^{1.5}\Big], \tag{22}$$

which is shown in Figure 2. Note that the maximum of the left stable branch of the scaled peel force ϕ has been normalized to unity by dividing f by $f_{max} = 280.8$, the maximum value of the peel force $f(v,V)$ curve on the left stable branch for $V = 1$. Since, v_{max}, at which the unstable branch starts, shifts as $\omega_u d$ changes with m, we have also scaled all the velocities with respect to $v_c = v_{max}/\omega_u d$. The range of pull velocities V in unscaled form ranges from $V = 0.4$ to 4. Thus, the curve corresponding to $V = 0.4$ in the scaled form would have the maximum value of ϕ less than unity and those corresponding to larger than $V = 1$ would have maximum at higher values than unity as shown in Figure 2.

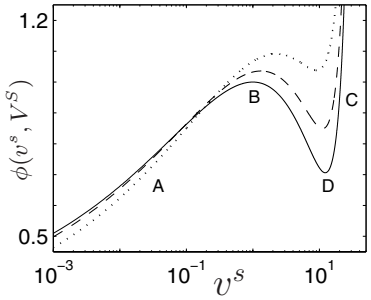

Fig. 2. Plots of $\phi(v^s, V^s)$ as a function of v^s for $V^s = 1.45$, 2.9, and 5.8 marked by solid, dashed and dotted curves respectively. ($V^s = 1.45$ refers low velocity regime and $V^s = 5.8$ high velocity regime.)

In scaled units, the equations of motion for $\alpha, \dot{\alpha}, X$ and v^s take the form

$$\ddot{\alpha} = \frac{1}{(1+\frac{l^s}{L^s}\sin\alpha)}\Bigg[-\frac{X}{R^s}+\frac{\phi(v^s,V^s)}{R^s(1+\frac{l^s}{L^s}\sin\alpha)} -\dot{\alpha}^2\Bigg(-\frac{R^s}{L^s}\left(\frac{l^s}{L^s}\sin\alpha\right)^2+\frac{l^s}{L^s}\cos\alpha\Bigg) -\frac{l^s}{L^s}\frac{C_f R^s\phi(v^s,V^s)\sin\alpha}{(1+\frac{l^s}{L^s}\sin\alpha)}\Bigg], \tag{23}$$

$$\dot{X} = (V^s - v^s)v_c + \frac{l^s}{L^s}R^s\sin\alpha\dot{\alpha}, \tag{24}$$

$$\dot{v}^s = \frac{1}{v_c(1+\frac{l^s}{L^s}\sin\alpha)}\Bigg[X^s-\frac{\phi(v^s,V^s)}{(1+\frac{l^s}{L^s}\sin\alpha)} +R^s\dot{\alpha}^2\Bigg(-\frac{R^s}{L^s}\left(\frac{l^s}{L^s}\sin\alpha\right)^2+\frac{l^s}{L^s}\cos\alpha\Bigg) -\frac{C_f\phi(v^s,V^s)(R^s\sin\alpha\frac{l^s}{L^s})^2}{(1+\frac{l^s}{L^s}\sin\alpha)}\Bigg] \tag{25}$$

and the over dots now denote differentiation with respect to τ.

The fixed point of equations (23)–(25) is given by $\alpha = 0$, $\dot{\alpha} = 0$, $X = \phi(v^s, V^s)$ and $v^s = V^s$. This point is stable for $\phi'(v^s, V^s) > 0$ and unstable for $\phi'(v^s, V^s) < 0$. As V^s is varied such that the sign of $\phi'(v^s, V^s)$ changes from negative to positive value, the system undergoes a Hopf bifurcation and a limit cycle appears. The limit cycle reflects the abrupt jumps between the two positive slope branches of the function $\phi'(v^s, V^s)$.

5 Results

Solutions obtained using the DAE algorithm as also the approximate solutions have been investigated in detail [9]. Our aim here is to report a comparative study of the DAE solutions with the ODE solutions for the entire range of parameters. We have solved the equations of motion (Eqs. (23)–(25)) by adaptive step size stiff differential solver (MATLAB package) and studied the dynamics of the system of equations for a wide range of values of the parameters. The results reported here are obtained after the long transients are omitted. Here, we report a few representative solutions for C_f and V^s keeping $R^s = 0.35$ and $l^s = 3.5$. We note that C_f depends linearly on the mass of the stretched tape m and inversely on the inertia of the roller I. It also depends on other parameters (f_{max} and k). We note that v_c represents the scaled critical velocity at which the unstable branch starts that depends on mass m for fixed f_{max} and k values. However, we note that the value of v_c is known once $f(v, V)$ is given.

Case 1: low mass limit

Here, we present some typical results. We begin by first showing that in the low mass limit (which refers to the mass of the tape), we essentially recover the DAE solutions reported in reference [9]. In this limit, i.e., low kinetic energy of the tape case, the right hand side of equation (8) is small, and thus

$$k\,u(1-\cos\theta) = F(1-\cos\theta) \approx f(v, V), \tag{26}$$

which is the algebraic constraint that makes the equations singular. Thus, one expects that the DAE solutions are reproduced for small mass which we have verified for the entire range of values of the roller inertia and pull velocity V^s. For all practical purposes, $m = 10^{-4}$ can be taken to be the low mass limit as the solutions are very similar to the DAE solutions. As an example of solutions for low mass limit, we first report the dynamics for $C_f = 0.788$, $V^s = 1.45$ (for which $v_c = 0.0008$) which represents low inertia of the roller($I = 10^{-5}$), low mass of the tape ($m = 10^{-4}$), and low pull velocity regime ($V = 1.0$) in terms of unscaled variables. Figures 3a–3d illustrates $\alpha(\tau)$, scaled force $X(\tau)$, scaled peel velocity $v^s(\tau)$, and the corresponding phase plots in $V^s - X$ plane. These plots are essentially similar to the DAE solution reported earlier (for example compare Figs. 3b and 3d with Figs. 4b and 4c in Ref. [9]). The saw tooth nature of the force has been observed in experiments.

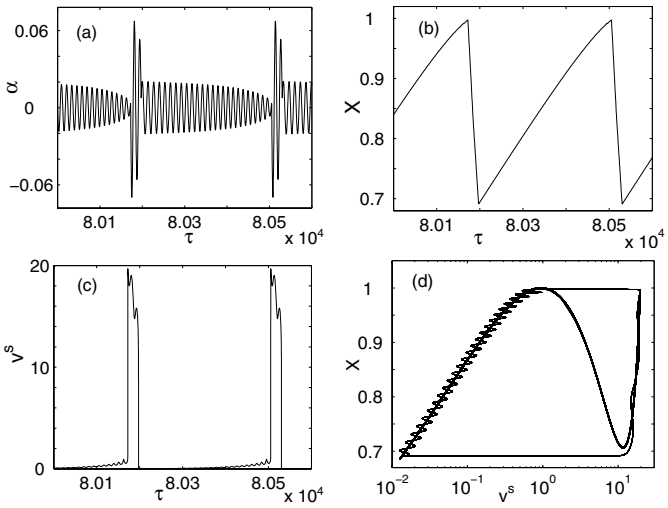

Fig. 3. Plot of $\alpha(\tau)$, $X(\tau)$, and $v^s(\tau)$ for $C_f = 0.788$ ($v_c = 0.0008$) corresponding to low roller inertia ($I = 10^{-5}$), low tape mass ($m = 10^{-4}$), and $V^s = 1.45$ (low pull velocity, $V = 1$). Phase space trajectory in the $v^s - X$ plane and corresponding $\phi(v^s, V^s)$ is shown by a bold line.

Case 2: high mass limit

As we go to the high mass limit, the inertial time scale corresponding to the kinetic energy of the stretched part of the tape increases. Much more complex dynamics emerges as a result of a competition between this additional time scale and other time scales present in the model equations. We shall illustrate the effect of increasing mass m on the dynamics for *high values of roller inertia*. For the sake of comparison, we first consider the case for high roller inertia ($I = 10^{-2}$) and low mass limit ($m = 10^{-4}$, i.e., DAE solution), for $C_f = 0.000788$ ($v_c = 0.0008$) and for low pull velocity $V^s = 1.45$. Plots of $\alpha(\tau)$, scaled force

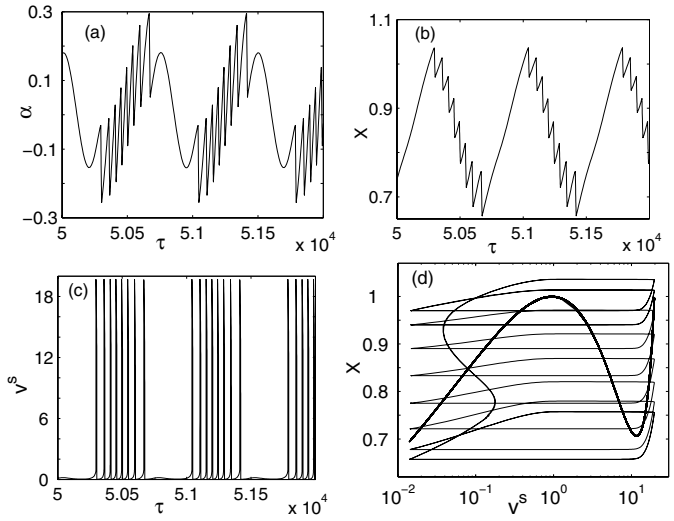

Fig. 4. Plot of $\alpha(\tau)$, $X(\tau)$, and $v^s(\tau)$ for $C_f = 0.000788$ ($v_c = 0.0008$) and $V^s = 1.45$. This corresponds to the high roller inertia ($I = 10^{-2}$), low tape mass ($m = 10^{-4}$), and low pull velocity ($V = 1$). Phase space trajectory in the $v^s - X$ plane and corresponding $\phi(v^s, V^s)$ is shown by a bold line.

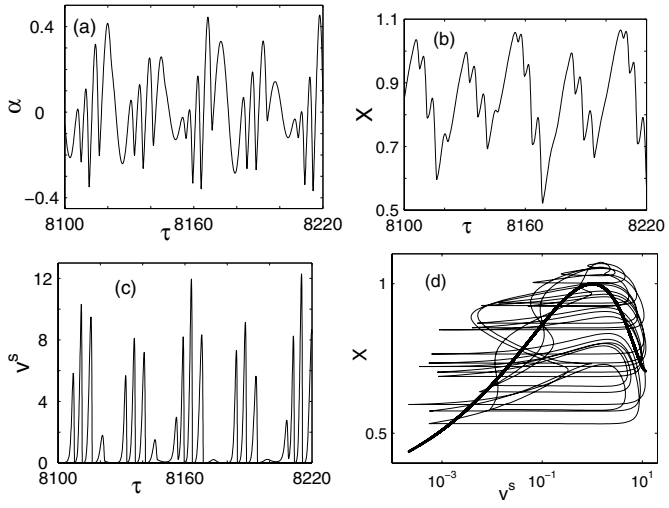

Fig. 5. Plot of $\alpha(\tau)$, $X(\tau)$, and $v^s(\tau)$ for $C_f = 0.788$ ($v_c = 0.024$) and $V^s = 1.45$. This corresponds to the high roller inertia ($I = 10^{-2}$), high tape mass ($m = 0.1$), and low pull velocity ($V = 1$). Phase space trajectory in the $v^s - X$ plane and corresponding $\phi(v^s, V^s)$ is shown by a bold line.

$X(\tau)$, scaled peel velocity $v^s(\tau)$, and the phase plots in $v^s - X$ plane are shown in Figures 4a–4d . This can be compared with high roller inertia ($I = 10^{-2}$) and high mass limit (0.1), i.e., keeping $C_f = 0.788$ ($v_c = 0.024$) and $V^s = 1.45$ illustrated in Figures 5a–5d for the same variables. It is evident from Figures 4a–4d and Figures 5a–5d that the influence of the additional time scale on all the variables is substantial. In particular, from Figure 5d, one can see that the orbit never jumps to the high velocity branch when the mass is large. More importantly, we note that the orbits spends substantial time in the region of the unstable branch. This is quite unusual. Such solutions are known as canard solutions [21]. Note also that the sharp changes in all the variables seen in the plot (Figs. 4a–4c) for the low mass limit (i.e., the DAE solutions) are rendered smooth for large mass case (Figs. 5a–5c).

To understand this, consider equation (8). It is clear that the inertial contribution from the stretched tape is the difference between the (given stationary) peel force and the dynamic force $F(t)$ which increases with mass. Further, rewriting equation (9), we get

$$m\dot{v} + m\ddot{u} + mR\cos\theta\,\ddot{\alpha} = mR\cos\alpha\,(\dot{\alpha})^2 \qquad (27)$$

where, we have used $\sin\theta\,\dot{\theta} \approx \cos\alpha\,\dot{\alpha}$. From this, it is clear that sum of the instantaneous peel force, the inertial force and that due to rotation arising from abrupt peeling has to be matched by a positive dissipation (right hand side). As shown in reference [9], for the zero mass case, i.e., the DAE solution jump abruptly when the limit of stability is reached. With increase in mass, increased levels of inertial contribution implies that the velocity has to be lesser than that corresponding to zero mass; in particular, the peel acceleration across the two branches has to be lesser which is the underlying cause of the orbit not visiting the high velocity branch of $f(v, V)$ or $\phi(v^s, V^s)$. Thus, the relaxational character wherein one finds regions of very slow changes followed by abrupt changes in the variable v [22,23], is removed by the inclusion of the inertial contribution.

Case 3: high roller inertia and high pull velocity

Increasing mass does not always increase the level of complexity of the solutions. As an example, Figures 6a–6d show plots for high pull velocity $V^s = 5.8$ case for $C_f = 0.000788$ ($v_c = 0.0008$) which corresponds to the low mass limit ($m = 10^{-4}$) and high roller inertia ($I = 10^{-2}$). It is clear that the force is nearly sinusoidal as demonstrated earlier which however has fine structure at the top and the bottom. This manifests in the form of a bunching of large amplitude velocity bursts. Note also that the dynamic force far exceeds the force values determined by force-velocity curve. In addition, the force-velocity phase plot also appears to be quite complex which can be shown to be chaotic. These features can be compared with the plots of Figures 7a–7d for the same variables for $C_f = 0.788$ ($v_c = 0.024$) for high mass limit ($m = 0.1$) and high roller inertia ($I = 10^{-2}$). While the ODE solution for small mass is similar to that of DAE which exhibits several sharp busts in velocity (Fig. 6c), the large mass case, $v^s(\tau)$ is surprisingly simple and is periodic (Fig. 7c). Indeed, the striking difference between the complex phase plot $v^s - X$ for low mass case (the DAE case) and the simple limit cycle plot for high mass is evident from Figures 6d and 7d respectively.

Finally, the complex nature of the orbit for certain values of parameter space can be quantified by calculating the Lyapunov spectrum. The irregular nature of the phase plot (Fig. 5d) is suggestive of chaotic dynamics is traditionally quantified by the existence of a positive Lyapunov exponent. We have calculated largest Lyapunov exponent

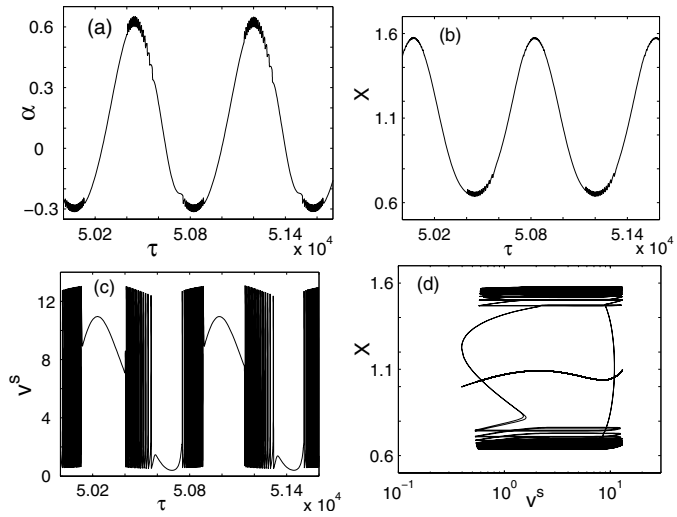

Fig. 6. Plot of $\alpha(\tau)$, $X(\tau)$, and $v^s(\tau)$ for $C_f = 0.000788$ ($v_c = 0.0008$) and $V^s = 5.8$. This corresponds to the high roller inertia ($I = 10^{-2}$), low tape mass ($m = 10^{-4}$), and high pull velocity ($V = 4$). Phase space trajectory in the $v^s - X$ plane and corresponding $\phi(v^s, V^s)$ is shown by a bold line.

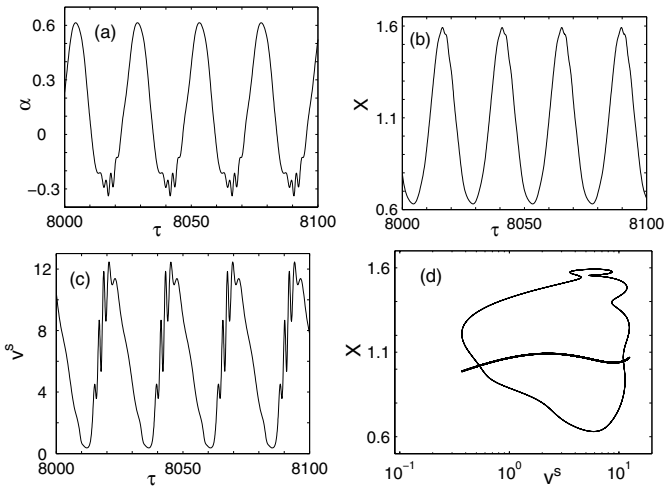

Fig. 7. Plot of $\alpha(\tau)$, $X(\tau)$, and $v^s(\tau)$ for $C_f = 0.788$ ($v_c = 0.024$) and $V^s = 5.8$. This corresponds to the high roller inertia ($I = 10^{-2}$), high tape mass ($m = 0.1$), and high pull velocity ($V = 4$). Phase space trajectory in the $v^s - X$ plane and corresponding $\phi(v^s, V^s)$ is shown by a bold line.

for these parameter values. The exponent turns out to be $\sim$0.06 s^{-1} (Fig. 8) which is a signature of a chaotic state. In contrast, the largest Lyapunov exponent for a periodic orbit (for instance Fig. 4d) turns out to be small $\sim$–0.0007 which can be considered to be essential zero as should be expected of a periodic orbit.

Another quantitative result that can be compared with experiment is the decreasing trend of the force drop magnitude with the pull velocity reported earlier (see Fig. 6 of [9]). The same trend is seen for the ODE model in the low mass limit both for low and high roller inertia cases. Figure 8b shows the monotonically decreasing trend of the

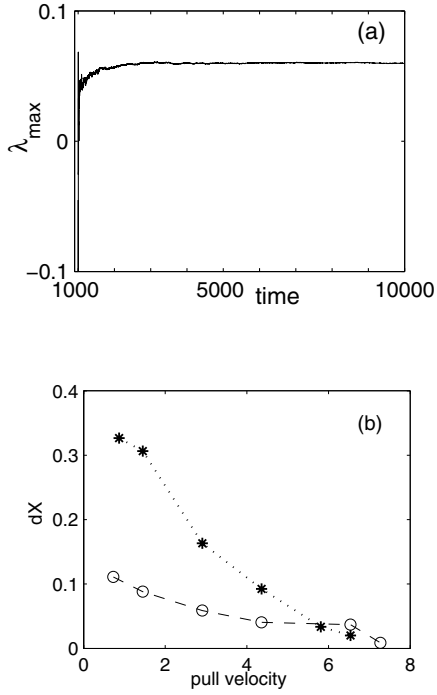

Fig. 8. (a) Largest Lyapunov exponent for $C_f = 0.788$ ($v_c = 0.024$) and $V^s = 1.45$ corresponding to high tape mass, high roller inertia and low pull velocity. (b) The plot shows the mean X drop ($\overline{\Delta X}$) as a function of the pull speed, V^s, for low mass limit. The dashed line corresponds to high roller inertia while the dotted line corresponds to small roller inertia.

average $\overline{\Delta X(\tau)}$ as V^s is increased, for both small and large roller inertia, a feature observed in experiments [1]. These two distinct behaviors are a result of the dynamization of $\phi(v, V)$ as in equation (22). However, for high mass limit, this result is not seen.

6 Summary and discussions

In summary, the two proposed methods, namely the differential algebraic algorithm and the set of ordinary differential equations resulting from the inclusion of the kinetic energy of the tape resolve the controversy surrounding the original model. These equations support dynamical jumps across the two stable branches of the peel force function as natural consequence of the equations of motion. The differential-algebraic algorithm, however, contains an arbitrary small parameter in perturbed mass matrix. As no physical meaning is attributable to this perturbed mass matrix, a re-examination of the derivation of the equations of motion shows that there is a missing time scale corresponding to the kinetic energy of the stretched tape. Once this term is included, it lifts the singular nature of the original model equations. We have presented a detailed comparative study of the regularized equations with that from differential algebraic equations. Solutions corresponding to the low mass limit of the tape agree with that provided by the DAE algorithm. There are host of other types of

solutions for large mass of the tape including chaotic and canard type of solutions not exhibited by the DAE model.

From a purely physical point of view, the complex dynamics observed in experiments on peeling could be attributed to the highly nonlinear nature of the peel force function and possibly due to different competing time scales. Apart from providing an algorithmic basis for obtaining dynamical jumps across the two stable branches of the peel force function (DAE), the next level of investigation (addition of kinetic energy of the tape) demonstrates the importance of including all the relevant variables and the associated time scales. This underscores the fact that just the negative force-velocity relation in itself cannot capture the full dynamics. It is worth pointing out that in two dimensions, discussions on relaxational oscillations show that the trajectories jump at the point of instability while the orbits stick and evolve slowly on the stable manifolds [22,23]. While this feature is not expected to hold in three dimensional phase space, the present approach shows that the addition of one more time scale can enhance the complexity of the dynamics substantially.

While the methodologies introduced resolve the controversy surrounding the model, comparison with experiments is limited only to qualitative features due to paucity of quantitative experimental results. Even so, our analysis shows that the average amplitudes of the drops in the pull force decreases as seen in experiments. Apart from this, several different waveforms observed in experiments such as the saw tooth, sinusoidal and irregular (chaotic) solutions are predicted by the model. Finally, we note that Maugis and Barquin [1] report irregular solutions, which they call chaotic (without any quantitative analysis) in a mid region of the instability. Assuming irregular wave forms correspond to chaotic solutions, in our model, they are also seen only a mid range of pull speeds. As the presence of chaotic solutions in mid range of instability is also common to the PLC effect, both in experiments [24–26] as well as in a model [17,27], some explanation is desirable. In both cases, the instability begins with a forward Hopf bifurcation and ends with a reverse Hopf bifurcation. The limit cycle emerging out of forward Hopf bifurcation needs to go through further bifurcations (to higher periodic states) before terminating in chaos. Similarly, as the instability is terminated by a reverse Hopf bifurcation, there should be periodic states beyond chaotic domain.

Our studies also show that the mass of the tape has a strong influence on the nature of the dynamics. For low pull velocities, and high I, the complexity increases, i.e., trajectories that are not chaotic for low mass become chaotic with increasing m. In some case, the orbits spend considerable time on the unstable branch never visiting the second branch. These orbits are reminiscent of canard [21] type of solutions. Clearly, these type of solutions emerge as a consequence of the new inertial time scale which essentially prevents the orbit from jumping to the stable branch at high velocity. In contrast, for high V, the trajectories that are chaotic for low m are rendered non chaotic with increase of m.

At a purely mathematical level, it appears that the present approach of introducing a time scale that lifts the singularity may have implications to the general class of differential-algebraic equations. It may be pointed here that with the addition of the kinetic energy term, the algebraic constraint is converted into a second order differential equation rather than a first order one, the latter would have been closer to the perturbed mass matrix in mathematical structure. Conversion of the algebraic constrain into a second order differential equation clearly cannot be universal. For instance, it is entirely possible that the missing physics could well be due to a damping mechanism which would make the differential equation to be first order. However, in cases where the differential algebraic equations of motion are derivable from Lagrangian or Hamiltonian formalism, it might be easier to recognize the missing time scale and therefore the form of differential equation resulting from the constrain equation.

The recognition of the missing physics has also other gains. The introduction of the kinetic energy of the stretched tape provides a mechanism for converting the potential energy stored in the stretched tape into kinetic energy and hence provides a basis for explaining acoustic emission during peeling which has so far remained ill understood. Indeed, we have extended the model to include spatial degrees of freedom along with an additional dissipation functional arising from rapid movement of the peel front. This extended model explains several features of acoustic emission observed in experiments [28].

GA would like to acknowledge the grant of Raja Ramana Fellowship and also support from BRNS Grant No. 2007/37/16/BRNS.

References

1. D. Maugis, M. Barquins, Adhesion 12, edited by K.W. Allen (Elsevier, London, 1988), p. 205; D. Maugis, CRNS Report. (1991)
2. M. Ciccotti, B. Giorgini, M. Barquins, Int. J. Adhes. Adhes. **18**, 35 (1998)
3. C. Gay, L. Leibler, Phys Today **52**, 48 (1999)
4. M. Barquins, M. Ciccotti, Int. J. Adhes. Adhes. **17**, 65 (1997)
5. M.C. Gandur, M.U. Kleinke, F.J. Galembeck, Adhes. Sci. Technol. **11**, 11 (1997)
6. D. Maugis, C.R. Acad. Sci. Paris **304**, 775 (1987)
7. D.C. Hong, S. Yue, Phys. Rev. Lett. **74**, 254 (1995)
8. D.C. Hong, Private communication
9. R. De, A. Maybhate, G. Ananthakrishna, Phys. Rev. E **70**, 46223 (2004)
10. E. Hairer, C. Lubich, M. Roche, *Numerical Solutions of Differential-algebraic Systems by Runge-Kutta Methods* (Springer-Verlag, Berlin, 1989)
11. R. De, G. Ananthakrishna, Phys. Rev. E **71**, R55201 (2005)
12. Actually, the kinetic energy at the peel front should be $\frac{m}{6}\dot{u}^2$. However, this does not alter the results
13. G. Ananthakrishna, R. De, Lecture Notes in Physics **705**, 423 (Springer, 2006)

14. B.N.J. Persson, *Sliding Friction: Physical Principles and Applications*, 2nd edn. (Springer, Heidelberg, 2000)
15. A. Portevin, F. Le Chatelier, C.R. Acad. Sci. Paris **176**, 507 (1923); F. Le Chatelier, Rev. de Métal. **6**, 914 (1909)
16. L.P. Kubin, C. Fressengeas, G. Ananthakrishna, *Collective Behaviour of Dislocations*, in *Dislocations in Solids*, edited by F.R.N. Nabarro, M.S. Deusbery (North-Holland, Amsterdam, 2002), Vol. 11, p. 101
17. G. Ananthakrishna, *Statistical and Dynamical Approaches to Collective Behaviour of Dislocations* in *Dislocations in Solids*, edited by J. Hirth, F.R.N. Nabarro (North-Holland, 2007), Vol. 13, p. 81; *Current Theoretical Approaches to Collective Behaviour of Dislocations*, Phys. Rep. **440**, 113 (2007)
18. L.P. Kubin, K. Chihab, Y. Estrin, Acta. Metall. **36**, 2707 (1988)
19. P.G. de Gennes, Langmuir **12**, 4497 (1996)
20. E.C.G. Sudarshan, N. Mukunda, *Classical Dynamics: A Modern Perspective* (John Wiley and Sons, New York, 1974)
21. M. Diener, The Mathematical Intelligence **6**, 38 (1984)
22. N. Minirsky, *Nonlinear Oscillations* (Van Nostrand, Princeton, New Jersey, 1962)
23. S.H. Strogatz, *Nonlinear Dynamics and Chaos* (Westview Press, 2000)
24. G. Ananthakrishna, M.C. Valsakumar, Phys. Lett. A **95**, 69 (1983)
25. G. Ananthakrishna et al., Phys. Rev. E **60**, 5455 (1999)
26. M.S. Bharathi, et al., Phys. Rev. Lett. **87**, 165508 (2001)
27. G. Ananthakrishna, M.S. Bharathi, Phys. Rev. E **70**, 26111 (2004)
28. R. De, G. Ananthakrishna, Phys. Rev. Lett. **97**, 165503 (2006)